Voltage staircase in a current-biased quantum-dot Josephson junction

D. O. Oriekhov ⦿, Y. Cheipesh ⦿, and C. W. J. Beenakker ⦿

Instituut-Lorentz, Universiteit Leiden, P.O. Box 9506, 2300 RA Leiden, The Netherlands

We calculate the current-voltage (I-V) characteristic of a Josephson junction containing a resonant level in the weakly coupled regime (resonance width small compared to the superconducting gap). The phase ϕ across the junction becomes time dependent in response to a DC current bias. Rabi oscillations in the Andreev levels produce a staircase I-V characteristic. The number of voltage steps counts the number of Rabi oscillations per 2π increment of ϕ, providing a way to probe the coherence of the qubit in the absence of any external AC driving. The phenomenology is the same as the Majorana-induced DC Shapiro steps in topological Josephson junctions of Choi *et al.* [Phys. Rev. B **102**, 140501(R) (2020)]—but now for a nontopological Andreev qubit.

I. INTRODUCTION

A single-mode weak link between superconductors supports a two-level system with a spacing that is adjustable via the superconducting phase difference [1,2]. Because Andreev reflection is at the origin of the phase sensitivity, the levels are called Andreev levels. Although their existence was implicit in early studies of the Josephson effect [3], the characteristic dependence $\propto \sqrt{1 - \tau \sin^2(\phi/2)}$ of the level spacing on the phase ϕ, with τ the transmission probability, was only identified [4] with the advent of nanostructures. The present interest in quantum information processing is driving theoretical [5,6] and experimental [7–10] studies of Andreev levels as qubits.

To assess the coherence of the qubit one would use AC microwave radiation of the two-level system and perform a time-resolved detection of the Rabi oscillations of the wave function [11]. In this paper we will show how a DC current I_{DC} and measurement of the time-averaged voltage $\bar{V}$ can be used to detect Rabi oscillations of an Andreev qubit: The staircase dependence of $\bar{V}$ on I_{DC} counts the number of Rabi oscillations per 2π increment of ϕ.

Our study is motivated by Choi, Calzona, and Trauzettel's report [12] of such a remarkable effect (dubbed "DC Shapiro steps") in a Majorana qubit—which is the building block of a topological quantum computer. As we will see, neither the unique topological properties of a Majorana qubit (its non-Abelian braiding and fusion rules) nor its specific symmetry class (class D, with broken time-reversal and spin-rotation symmetry) are needed, a similar phenomenology can be found in a nontopological Andreev qubit with preserved symmetries (class CI).

The outline of this paper is as follows. In Sec. II we present the model of the weak link that we will consider: a quantum dot connecting two superconductors with a tunnel rate Γ small compared to the superconducting gap Δ_0. Such a Josephson junction has been extensively studied [13–15] in the regime where Coulomb charging and the Kondo effect govern the charge transfer [16–18]. We will assume the charging energy is small and treat the quasiparticles as noninteracting.

The dynamics of a current-biased, resistively shunted quantum-dot Josephson junction is studied in Secs. III and IV. The voltage staircase is shown in Fig. 3 and the one-to-one relationship with the number of Rabi oscillations is in Fig. 6. In the concluding section, Sec. V, we will explain why the substitution of the quantum dot by a quantum point contact will remove the voltage staircase.

II. ANDREEV LEVEL HAMILTONIAN

We consider the Josephson junction shown in Fig. 1, consisting of a quantum dot in the normal state (N) coupled via a tunnel barrier to superconductors (S) at the left and right, with pair potentials $\Delta_0 e^{i\phi_L}$ and $\Delta_0 e^{i\phi_R}$. We focus on the weakly coupled regime, when the tunnel rates Γ_L and Γ_R through the barrier are small compared to Δ_0.

We assume that the fully isolated quantum dot has a single electronic energy level E_0 within an energy range $\Gamma = \Gamma_L + \Gamma_R$ from the Fermi energy μ. The normal-state conductance G_N is then given by the Breit-Wigner formula

$$G_N = \frac{2e^2}{h}\tau_{BW}, \quad \tau_{BW} = \frac{\Gamma_L \Gamma_R}{(E_0 - \mu)^2 + \frac{1}{4}\Gamma^2}. \quad (2.1)$$

Coupling of electrons and holes by Andreev reflection from the superconductor produces a pair of Andreev levels at energies $\pm E_A(\phi)$, dependent on the phase difference $\phi = \phi_L - \phi_R$ between the left and right superconductors.

A simplifying assumption of our analysis is that the Coulomb charging energy U is small compared to Γ and can be neglected. If U is larger than Γ but still smaller than Δ_0, the main effect of the charging energy is a shift of the energy level of the dot, $E_0 \mapsto E_0 + U/2$. Provided $E_0 > 0$ the ground state remains a spin singlet [19], and we do not expect a qualitative change in our results. If U becomes larger than Δ_0 the supercurrent is reduced by a factor Γ/Δ_0 because tunneling of a Cooper pair into the quantum dot is suppressed [16–18].

To describe the nonequilibrium dynamics of the junction we seek the effective low-energy Hamiltonian of time-dependent Andreev levels. This requires information not only
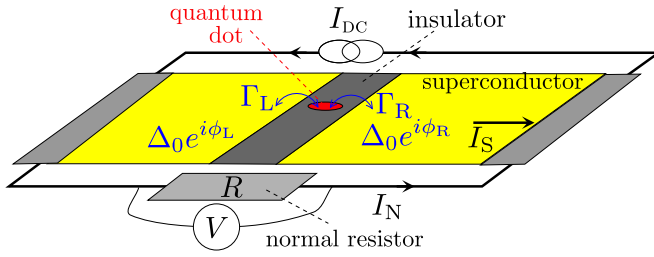
FIG. 1. Current-biased, resistively shunted Josephson junction, formed out of two superconductors (phases ϕ_L and ϕ_R) separated by an insulator containing a quantum dot (tunnel rates Γ_L and Γ_R from the left and from the right). The superconducting phases become time dependent when a voltage difference V develops in response to a DC current I_{DC}.

on the eigenvalues but also on the eigenfunctions. In Secs. II A and II B we summarize results from Refs. [19–22] for the time-independent situation, which we need as input for the dynamical study starting from Sec. II C.

A. Andreev levels

For an arbitrary ratio of Γ and Δ_0 the energies of the Andreev levels are equal to the two real solutions $\pm E_A$ of the equation [20,21]

$$\Omega(E, \phi) + \Gamma E^2 \sqrt{\Delta_0^2 - E^2} = 0, \qquad (2.2)$$

with

$$\Omega(E, \phi) = (\Delta_0^2 - E^2)\left[E^2 - (E_0 - \mu)^2 - \tfrac{1}{4}\Gamma^2\right] + \Delta_0^2 \Gamma_L \Gamma_R \sin^2(\phi/2). \qquad (2.3)$$

In the weak-coupling regime $\Gamma \ll \Delta_0$, assuming also $|E_0 - \mu| \ll \Delta_0$, this reduces to

$$E_A = \Delta_{\text{eff}} \sqrt{1 - \tau_{\text{BW}} \sin^2(\phi/2)},$$
$$\Delta_{\text{eff}} = \sqrt{(E_0 - \mu)^2 + \tfrac{1}{4}\Gamma^2}, \qquad (2.4)$$

no longer dependent on Δ_0. The two Andreev levels have an avoided crossing at $\phi = \pi$, separated by an energy

$$\delta E = \sqrt{4(E_0 - \mu)^2 + (\Gamma_L - \Gamma_R)^2} \qquad (2.5)$$

(see Fig. 2).

The equilibrium supercurrent, at temperatures $k_B T \ll \Gamma$, is given by

$$I_{\text{eq}}(\phi) = -\frac{2e}{\hbar}\frac{dE_A}{d\phi} = \frac{e\Gamma_L \Gamma_R \sin\phi}{2\hbar E_A(\phi)}, \qquad (2.6)$$

with critical current (maximal supercurrent)

$$I_c = \frac{e}{\hbar}\left[\sqrt{(E_0 - \mu)^2 + \tfrac{1}{4}\Gamma^2} - \sqrt{(E_0 - \mu)^2 + \tfrac{1}{4}\Gamma^2 - \Gamma_L \Gamma_R}\right]. \qquad (2.7)$$

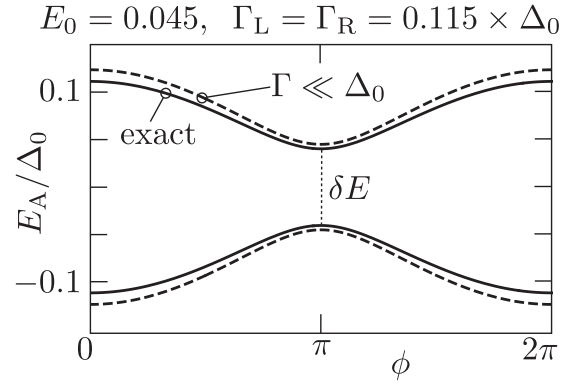There is no contribution from the continuous spectrum in the weak-coupling regime [20].

FIG. 2. Andreev levels $\pm E_A(\phi)$ according to the full expression (2.2) (solid curve) and in the weak-coupling approximation (2.4) (dashed curve, parameters $E_0 = 0.045$, $\mu = 0$, $\Gamma_L = \Gamma_R = 0.115$, all in units of Δ_0).

B. Effective Hamiltonian: Time-independent phase

For time-independent phases the effective low-energy Hamiltonian in the weak-coupling regime $\Gamma \ll \Delta_0$ follows from second-order perturbation theory [19,22],

$$H = -\tfrac{1}{2}(e^{i\phi_L}\Gamma_L + e^{i\phi_R}\Gamma_R)a_\uparrow^\dagger a_\downarrow^\dagger + \text{H.c.}$$
$$+ (E_0 - \mu)(a_\uparrow^\dagger a_\uparrow + a_\downarrow^\dagger a_\downarrow). \qquad (2.8)$$

Here, $a_\uparrow$ and $a_\downarrow$ are the fermionic annihilation operators of a spin-up or spin-down electron in the quantum dot.

The corresponding Bogoliubov–de Gennes (BdG) Hamiltonian $\mathcal{H}$ is a 4×4 matrix contracted with the spinors $\Psi = (a_\uparrow, -a_\downarrow^\dagger, a_\downarrow, -a_\uparrow^\dagger)$ and $\Psi^\dagger$,

$$H = \tfrac{1}{2}\Psi^\dagger \mathcal{H} \Psi + E_0 - \mu. \qquad (2.9)$$

It is block-diagonal, so we only need to consider one 2×2 block, given by

$$\mathcal{H} = \begin{pmatrix} E_0 - \mu & \tfrac{1}{2}e^{i\phi_L}\Gamma_L + \tfrac{1}{2}e^{i\phi_R}\Gamma_R \\ \tfrac{1}{2}e^{-i\phi_L}\Gamma_L + \tfrac{1}{2}e^{-i\phi_R}\Gamma_R & \mu - E_0 \end{pmatrix}. \qquad (2.10)$$

One readily checks that the eigenvalues $\pm E_A$ of $\mathcal{H}$ are given by Eq. (2.4).

C. Effective Hamiltonian: Time-dependent phase

When the left and right superconductors are at different voltages $\pm V/2$, the superconducting phase becomes time dependent. We choose a gauge such that $\phi_L(t) = \phi(t)/2$, $\phi_R(t) = -\phi(t)/2$, evolving in time according to the Josephson relation

$$\dot\phi \equiv d\phi/dt = (2e/\hbar)V. \qquad (2.11)$$

The voltage bias imposes an electrical potential on the quantum dot, which shifts μ by an amount $\tfrac{1}{2}\gamma eV$ with $\gamma = (\Gamma_L - \Gamma_R)/\Gamma$.

The time-dependent BdG Hamiltonian then becomes

$$\mathcal{H}(t) = \begin{pmatrix} E_0 - \mu - \frac{1}{4}\hbar\gamma\dot{\phi}(t) & \frac{1}{2}e^{i\phi(t)/2}\Gamma_L + \frac{1}{2}e^{-i\phi(t)/2}\Gamma_R \\ \frac{1}{2}e^{-i\phi(t)/2}\Gamma_L + \frac{1}{2}e^{i\phi(t)/2}\Gamma_R & \mu - E_0 + \frac{1}{4}\hbar\gamma\dot{\phi}(t) \end{pmatrix}$$

$$= \left[E_0 - \mu - \tfrac{1}{4}\hbar\gamma\dot{\phi}(t)\right]\sigma_z + \tfrac{1}{2}\Gamma\left[\sigma_x \cos\tfrac{1}{2}\phi(t) - \gamma\sigma_y \sin\tfrac{1}{2}\phi(t)\right]. \qquad (2.12)$$

The Pauli matrices act on the electron-hole degree of freedom. The corresponding current operator is given by

$$I(t) = \frac{2e}{\hbar}\frac{\partial}{\partial\phi}\mathcal{H}(t) = -\frac{e\Gamma}{2\hbar}\left[\sigma_x \sin\frac{1}{2}\phi(t) + \gamma\sigma_y \cos\frac{1}{2}\phi(t)\right]. \qquad (2.13)$$

Notice that the Hamiltonian (2.12) depends both on $\phi(t)$ and on $\dot{\phi}(t)$, unless $\Gamma_L = \Gamma_R$. It is possible to remove the $\dot{\phi}$ dependence by a time-dependent unitary transformation [23], but since this does not simplify our subsequent calculations we will keep the form (2.12).

III. VOLTAGE STAIRCASE

As shown in Fig. 1, a time-independent current bias I_{DC} is driven partially through the Josephson junction, as a supercurrent $I_S(t)$, and partially through a parallel resistor R as a normal current $I_N(t) = V(t)/R$. Substitution of the Josephson relation (2.11) gives the differential equation

$$d\phi(t)/dt = (2eR/\hbar)[I_{DC} - I_S(t)]. \qquad (3.1)$$

Here, we neglect the junction capacitance (overdamped regime of a resistively shunted Josephson junction) [24]. We work in the low-temperature regime, $k_B T \ll \Delta_0$, so that we may ignore thermal fluctuations of the phase due to the voltage noise over the external resistance [25].

The supercurrent is obtained from the expectation value

$$I_S(t) = \langle\Psi(t)|I(t)|\Psi(t)\rangle, \qquad (3.2)$$

where the current operator is given by Eq. (2.13) and the wave function evolves according to the Schrödinger equation

$$i\hbar\frac{d}{dt}|\Psi(t)\rangle = \mathcal{H}(t)|\Psi(t)\rangle. \qquad (3.3)$$

As initial condition we take $\phi(0) = 0$ and $|\Psi(0)\rangle$ the eigenstate of the Andreev level at $-E_A$ for $\phi = 0$. The DC current I_{DC} is increased slowly from zero to some maximal value and then slowly decreased back to zero. The I-V characteristic is obtained by averaging $V(t)$ over a moving time window in which I_{DC} is approximately constant.

Results of this numerical integration are shown in Fig. 3. We observe a staircase dependence of $\bar{V}$ on I_{DC}. The nonzero voltage appears at the critical current (2.7) for the up sweep and disappears at a slightly lower current for the down sweep. (A similar difference between switching current and retrapping current was found for the Majorana qubit [27].) The voltage steps at $I_{DC} > I_c$ also show hysteresis: The voltage jump up happens at larger DC current than the voltage jump down. (This hysteresis also appears in the Majorana qubit; see the Appendix.)

IV. ANDREEV QUBIT DYNAMICS

The voltage staircase of Fig. 3 is a signature of Rabi oscillations of the Andreev qubit formed by the two Andreev levels in the Josephson junction, in much the same way that the voltage steps of Ref. [12] were driven by Rabi oscillations of a Majorana qubit. Let us investigate the Andreev qubit dynamics.

A. Adiabatic evolution

In the adiabatic regime of a slow driving, $\hbar\dot{\phi} \ll \delta E$, transitions between the Andreev levels can be neglected and the phase evolves in time as an overdamped classical particle,
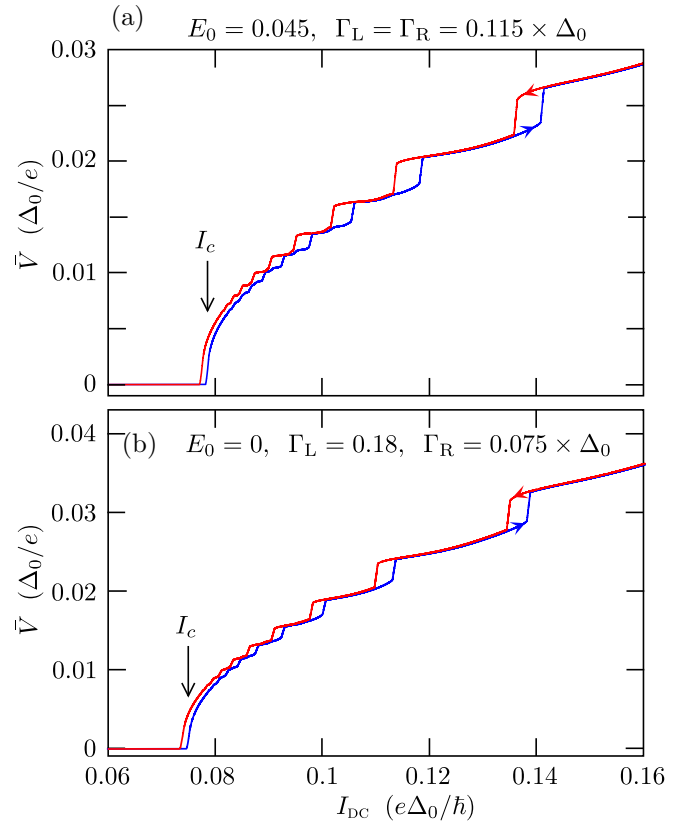
$$\dot{\phi} + dU_A/d\phi = 0, \qquad (4.1)$$

FIG. 3. Current-voltage characteristic of the quantum-dot Josephson junction, for two different parameter sets [26]. The blue curve is for increasing DC current, the red curve for decreasing current. The Andreev levels in Fig. 2 correspond to the parameters in (a). The critical current (2.7) is indicated by the black arrow.
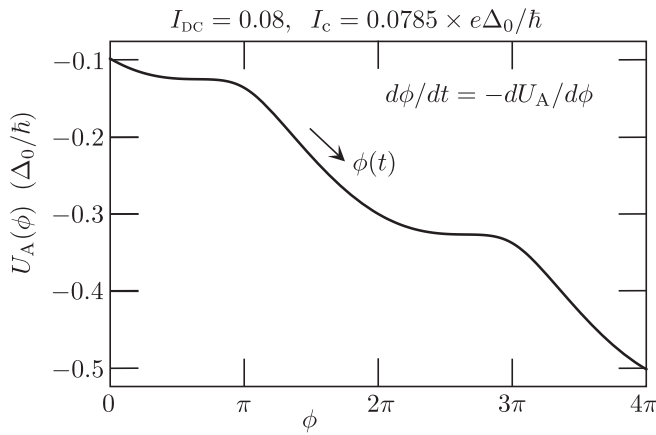
FIG. 4. Washboard potential (4.2) that governs the time depen-
dence of the superconducting phase in the adiabatic limit. The curve
is plotted for the junction parameters of Figs. 2 and 3(a), at a value
of I_{DC} slightly above the critical current I_c.

moving in the "washboard potential" [24]

$$U_A(\phi) = -(2eR/\hbar)[\phi I_{DC} + (2e/\hbar)E_A(\phi)], \quad (4.2)$$

plotted in Fig. 4.

The time dependence of the phase resulting from integra-
tion of Eq. (4.1) is shown in Fig. 5(a). Figure 5(b) tracks
the adiabatic dynamics of the Andreev qubit, by plotting
the Bloch sphere coordinates $\boldsymbol{R} = (X, Y, Z)$, with $R_\alpha(t) =$
$\langle \Psi(t)|\sigma_\alpha|\Psi(t)\rangle$. The qubit dynamics is 4π-periodic in ϕ,
because the Hamiltonian (2.12) is 4π-periodic: When ϕ is

increased by 2π, one has $\mathcal{H} \mapsto \sigma_z \mathcal{H} \sigma_z$, so on the Bloch sphere
the qubit is rotated by π around the z axis ($X \mapsto -X$, $Y \mapsto$
$-Y$). The full spectrum is a 2π-periodic function of ϕ, in
particular the Josephson current (2.6) is 2π-periodic—this
nontopological Josephson junction does not exhibit the 4π-
periodic Josephson effect that is the hallmark of a topological
superconductor.

B. Pulsed Rabi oscillations

Figures 5(c) and 5(d) show the full nonadiabatic dynamics,
obtained by integration of Eq. (3.3) for the same parameter
set as in Figs. 5(a) and 5(b). Transitions between the Andreev
levels produce pronounced Rabi oscillations of the qubit, also
visible as small oscillations in $\phi(t)$.

Because the supercurrent carried by the two Andreev levels
$\pm E_A$ has the opposite sign, the interlevel transitions reduce I_S,
thereby increasing $I_N = I_{DC} - I_S$ and hence $\bar{V}$. This is evident
from Fig. 5(c), which shows that the first 2π increment of ϕ,
without interlevel transitions, takes a time $\delta t \approx 1000 \, \hbar/\Delta_0$,
while the second 2π increment, with Rabi oscillations, only
takes a time $\delta t = 700$. The average voltage $\bar{V} \simeq 2\pi/\delta t$ is
therefore increased by a factor $10/7$ because of the interlevel
transitions.

The Rabi oscillations are pulsed: They appear abruptly
when ϕ crosses $(2n-1)\pi$ and increases rapidly to $2n\pi$,
which is the steepest part of the washboard potential (see
Fig. 4).

To estimate the Rabi frequency we substitute $\Psi(t) =$
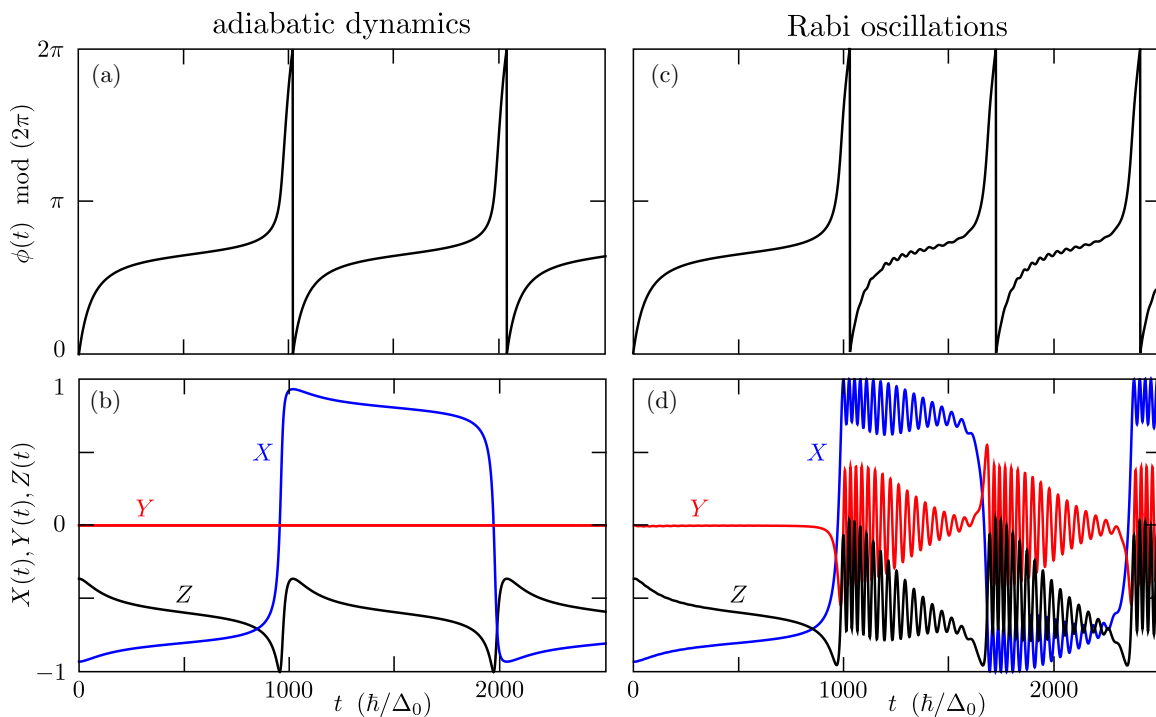$[u(t)e^{i\phi(t)/4}, v(t)e^{-i\phi(t)/4}]$ in the Schrödinger equation (3.3)

FIG. 5. Time dependence of the superconducting phase (top row) and of the Bloch sphere coordinates of the Andreev qubit (bottom row),
in the adiabatic limit (left column) and in the nonadiabatic regime in which transitions between the Andreev levels produce Rabi oscillations
of the qubit (right column). The junction parameters are those of Fig. 3(a), at $I_{DC} = 0.08 \, e\Delta_0/\hbar$. The wave function was initialized as an
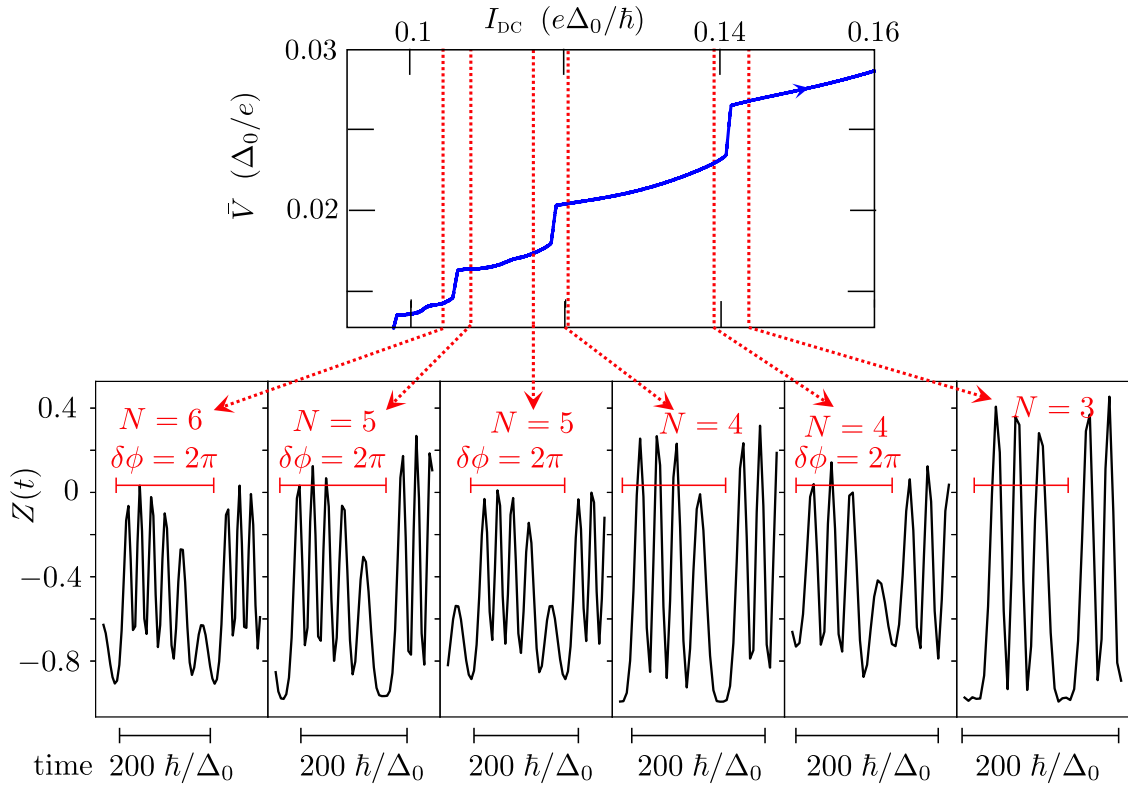eigenstate of the lowest Andreev level $-E_A(0)$ at $t = 0$.

FIG. 6. Top panel: Portion of the *I-V* characteristic from Fig. 3(a), with red dotted lines into the bottom panels to show how the voltage steps line up with the change in the number N of Rabi oscillations of the qubit in a 2π phase increment $\delta\phi$.

and make the rotating wave approximation, discarding rapidly oscillating terms $\propto e^{i\phi(t)}$:

$$i\hbar\dot{u}(t) = \left[E_0 - \mu + \tfrac{1}{2}eV(t)\right]u(t) + \tfrac{1}{4}\Gamma v(t),$$
$$i\hbar\dot{v}(t) = -\left[E_0 - \mu + \tfrac{1}{2}eV(t)\right]v(t) + \tfrac{1}{4}\Gamma u(t). \quad (4.3)$$

(We have set $\Gamma_{\mathrm{L}} = \Gamma_{\mathrm{R}}$ for simplicity.) If we further neglect the slow time dependence of the voltage, we obtain oscillations $\propto \sin^2 \omega_{\mathrm{R}} t$ of the Bloch vector components X, Y, Z with Rabi frequency

$$\hbar\omega_{\mathrm{R}} = \sqrt{\left(E_0 - \mu + \tfrac{1}{2}eV\right)^2 + (\Gamma/4)^2}. \quad (4.4)$$

The oscillations in Fig. 5(d) near $t = 1000 \times \hbar/\Delta_0$ have a period of $35\,\hbar/\Delta_0$, while $T_{\mathrm{R}} = \pi/\omega_{\mathrm{R}} = 40\,\hbar/\Delta_0$ if we set $V = RI_{\mathrm{DC}}$, in reasonable agreement.

C. Voltage steps count Rabi oscillations

The key discovery of Ref. [12] is that steps in the time-averaged voltage track the change in the number of Rabi oscillations of the Majorana qubit per 2π increment of the superconducting phase. Figure 6 shows the same correspondence for the Andreev qubit.

If we estimate the duration δt of a 2π phase increment by the product of the number N of Rabi oscillations and the Rabi period T_{R}, we obtain the estimate $(2e/\hbar)\bar{V} = 2\pi/\delta t \simeq 2\omega_{\mathrm{R}}/N$. A stepwise decrease of N with increasing I_{DC} would then produce a stepwise increase of $\bar{V}$. This argument is suggestive, but does not explain the sharpness of the steps. We

have no quantitative analytical derivation for why the steps are as sharp as they appear in the numerics.

V. DISCUSSION

Two lessons learned from this study are as follows: (1) Rabi oscillations of an Andreev qubit can be counted "one by one" without either requiring time-resolved detection or AC driving. (2) The voltage staircase phenomenology of Ref. [12] does not need a topological Majorana qubit — it exists in a conventional Andreev qubit.

We worked in the weak-coupling regime $\Gamma \ll \Delta_0$ because it simplifies the calculations, but also for a physics reason: The voltage staircase is suppressed when Γ becomes larger than Δ_0, due to a well-known decoherence mechanism [25,28]: equilibration of the Andreev levels $\pm E_{\mathrm{A}}(\phi)$ with the continuous spectrum at $|E| > \Delta_0$ when ϕ crosses an integer multiple of 2π. Let us discuss this in a bit more detail.

For $\Gamma \gg \Delta_0$ the Andreev levels are given by

$$E_{\mathrm{A}} = \Delta_0\sqrt{1 - \tau_{\mathrm{BW}} \sin^2(\phi/2)}, \quad (5.1)$$

according to Eq. (2.2), with τ_{BW} the Breit-Wigner transmission probability (2.1). The difference with the weak-coupling result (2.4) is that the reduced gap Δ_{eff} has been replaced by the true gap Δ_0. This means the Andreev level merges with the superconducting continuum whenever $\phi = 0$ modulo 2π. As the phase evolves in time in response to the current bias, each 2π phase increment will restart from an equilibrium distribution.

Now if we examine Figs. 5(c) and 5(d), we see that the Rabi oscillations are pulsed by the rapid increase of the phase in the $(\pi, 2\pi)$ interval, and only fully develop in the $(2\pi, 3\pi)$ interval. Equilibration at $\phi = 2\pi$ will restart the cycle from $t = 0$, suppressing the Rabi oscillations and hence the voltage staircase.

For the same reason a superconducting quantum point contact will not show the voltage staircase: Its Andreev levels also reconnect with the superconducting continuum at $\phi = 0$ modulo 2π.

This argument points to one difference in the Majorana versus Andreev phenomenology of the voltage staircase: A topological Josephson junction needs to be magnetic in order to prevent the equilibration of the Majorana modes with the continuum at $\phi = 0$ modulo 2π [29]. In a nontopological quantum-dot Josephson junction this can achieved without breaking time-reversal symmetry.

As a topic for further research, it would be worthwhile to see if the voltage staircase can be used to count the number of Rabi oscillations over multiple 2π phase increments, since that would provide additional information on the coherence time of the qubit. This could involve the constructive interference of Landau-Zener transitions at $\phi = \pi, 3\pi, \dots$ [30].

APPENDIX: HYSTERESIS OF THE VOLTAGE STAIRCASE FOR THE MAJORANA QUBIT

The voltage staircase of the Andreev qubit is hysteretic, and the steps appear at a higher current for the up sweep than for the down sweep. No hysteresis was reported in Ref. [12],
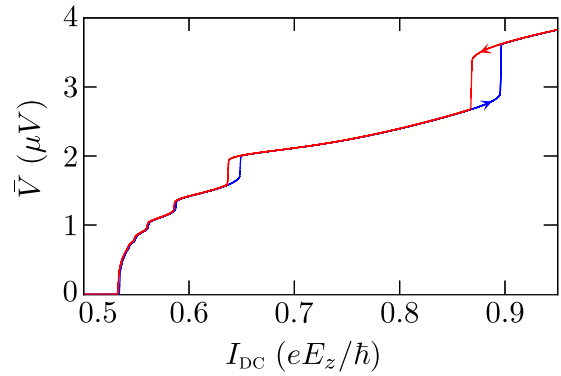

FIG. 7. Hysteretic voltage staircase of the Majorana Josephson junction, for the parameters of Ref. [12], Fig. 3. The blue curve is for increasing DC current, the red curve for decreasing current. (The voltage $\bar{V}$ is averaged over a time window δt such that $\delta t \times dI_{\mathrm{DC}}/dt = 10^{-3} \, eE_z/\hbar$.)

so here we show that it is present for the Majorana qubit as well.

Instead of Eqs. (2.12) and (2.13), one has for the Majorana qubit the time-dependent Hamiltonian

$$\mathcal{H}(t) = E_x \sigma_x + E_z \sigma_z \cos \tfrac{1}{2}\phi(t), \tag{A1}$$

and current operator

$$I(t) = \frac{2e}{\hbar} \frac{\partial}{\partial \phi} \mathcal{H}(t) = -\frac{eE_z}{\hbar} \sigma_z \sin \frac{1}{2}\phi(t). \tag{A2}$$

The Pauli matrices act on the fermion parity of two pairs of Majorana zero modes, such that σ_x flips the even-even parity state into the odd-odd parity state, while σ_z changes the sign of the odd-odd parity state. While the physical origin of the Majorana coupling terms is different from the Andreev qubit, mathematically the Hamiltonian (A1) is equivalent to Eq. (2.12) in the symmetric case $\Gamma_L = \Gamma_R$. (Switch $\sigma_x \leftrightarrow \sigma_z$ by a unitary transformation and replace $E_x \mapsto E_0 - \mu$ and $E_z \mapsto \Gamma/2$.)

In Fig. 7 we show the hysteretic voltage staircase, for the same parameters $E_z = 5 \, \mu\mathrm{eV}$, $E_x/E_z = 0.67$, and $R = 0.827 \, \hbar/e^2$ as in Ref. [12].

[1] A. Furusaki and M. Tsukada, Current-carrying states in Josephson junctions, Phys. Rev. B **43**, 10164 (1991).

[2] C. W. J. Beenakker and H. van Houten, Josephson Current through a Superconducting Quantum Point Contact Shorter than the Coherence Length, Phys. Rev. Lett. **66**, 3056 (1991).

[3] I. O. Kulik and A. N. Omel'yanchuk, Properties of superconducting microbridges in the pure limit, Sov. J. Low Temp. Phys. **3**, 459 (1977).

[4] C. W. J. Beenakker, Universal Limit of Critical-Current Fluctuations in Mesoscopic Josephson Junctions, Phys. Rev. Lett. **67**, 3836 (1991).

[5] A. Zazunov, V. S. Shumeiko, E. N. Bratus', J. Lantz, and G. Wendin, Andreev Level Qubit, Phys. Rev. Lett. **90**, 087003 (2003).

[6] N. M. Chtchelkatchev and Yu. V. Nazarov, Andreev Quantum Dots for Spin Manipulation, Phys. Rev. Lett. **90**, 226806 (2003).

[7] L. Bretheau, Ç. Ö. Girit, H. Pothier, D. Esteve, and C. Urbina, Exciting Andreev pairs in a superconducting atomic contact, Nature (London) **499**, 312 (2013).

[8] C. Janvier, L. Tosi, L. Bretheau, Ç. Ö. Girit, M. Stern, P. Bertet, P. Joyez, D. Vion, D. Esteve, M. F. Goffman, H. Pothier, and C. Urbina, Coherent manipulation of Andreev states in superconducting atomic contacts, Science **349**, 1199 (2015).

[9] M. Hays, G. de Lange, K. Serniak, D. J. van Woerkom, D. Bouman, P. Krogstrup, J. Nygård, A. Geresdi, and M. H. Devoret, Direct Microwave Measurement of Andreev-Bound-State Dynamics in a Proximitized Semiconducting Nanowire, Phys. Rev. Lett. **121**, 047001 (2018).

[10] M. Hays, V. Fatemi, D. Bouman, J. Cerrillo, S. Diamond, K. Serniak, T. Connolly, P. Krogstrup, J. Nygård, A. Levy Yeyati, A. Geresdi, and M. H. Devoret, Coherent manipulation of an Andreev spin qubit, arXiv:2101.06701.

[11] F. S. Bergeret, P. Virtanen, A. Ozaeta, T. T. Heikkilä, and J. C. Cuevas, Supercurrent and Andreev bound state dynamics in superconducting quantum point contacts under microwave irradiation, Phys. Rev. B **84**, 054504 (2011).

[12] S.-J. Choi, A. Calzona, and B. Trauzettel, Majorana-induced DC Shapiro steps in topological Josephson junctions, Phys. Rev. B **102**, 140501(R) (2020).

[13] A. Martín-Rodero and A. Levy Yeyati, Josephson and Andreev transport through quantum dots, Adv. Phys. **60**, 899 (2011).

[14] V. Meden, The Anderson–Josephson quantum dot—a theory perspective, J. Phys.: Condens. Matter **31**, 163001 (2019).

[15] A. Levy Yeyati, A. Martín-Rodero, and E. Vecino, Nonequilibrium Dynamics of Andreev States in the Kondo Regime, Phys. Rev. Lett. **91**, 266802 (2003).

[16] L. I. Glazman and K. A. Matveev, Resonant Josephson current through Kondo impurities in a tunnel barrier, Pis'ma Zh. Eksp. Teor. Fiz. **49**, 570 (1989) [JETP Lett. **49**, 659 (1989)].

[17] B. I. Spivak and S. A. Kivelson, Negative local superfluid densities: The difference between dirty superconductors and dirty Bose liquids, Phys. Rev. B **43**, 3740 (1991).

[18] T. Novotný, A. Rossini, and K. Flensberg, Josephson current through a molecular transistor in a dissipative environment, Phys. Rev. B **72**, 224502 (2005).

[19] T. Meng, S. Florens, and P. Simon, Self-consistent description of Andreev bound states in Josephson quantum dot devices, Phys. Rev. B **79**, 224521 (2009).

[20] C. W. J. Beenakker and H. van Houten, Resonant Josephson current through a quantum dot, in *Single-Electron Tunneling and Mesoscopic Devices*, edited by H. Koch and H. Lübbig, Springer Series in Electronics and Photonics Vol. 31 (Springer, Berlin, 1992), pp. 175–179.

[21] I. A. Devyatov and M. Yu. Kupriyanov, Resonant Josephson tunneling through S-I-S junctions of arbitrary size, JETP **85**, 189 (1997).

[22] P. Recher, Yu. V. Nazarov, and L. P. Kouwenhoven, The Josephson Light-Emitting Diode, Phys. Rev. Lett. **104**, 156802 (2010).

[23] The time-dependent unitary transformation $\Psi \mapsto U^{\dagger}\Psi$, $\mathcal{H} \mapsto U^{\dagger}\mathcal{H}U - i\hbar U^{\dagger}dU/dt$ with $U(t) = e^{i\sigma_z \gamma \phi(t)/4}$ removes the $\dot{\phi}$ term from the Hamiltonian (2.12). The γ parameter then appears in the superconducting phases, $\phi_{\mathrm{L}} = \frac{1}{2}(1 - \gamma)\phi$, $\phi_{\mathrm{R}} = -\frac{1}{2}(1 + \gamma)\phi$.

[24] M. Tinkham, *Introduction to Superconductivity* (Dover, New York, 2004).

[25] D. V. Averin, A. Bardas, and H. T. Imam, Resistively shunted superconducting quantum point contacts, Phys. Rev. B **58**, 11165 (1998).

[26] The parameters E_0, Γ_{L}, Γ_{R} used in Fig. 3 are listed in each panel; additional parameters: $\mu = 0$ in both panels, $R = 0.20$ and $0.25\hbar/e^2$ in Figs. 3(a) and 3(b), respectively. The voltage $\bar{V}$ is averaged over a time window δt such that $\delta t \times dI_{\mathrm{DC}}/dt = 6.3 \times 10^{-4}e\Delta_0/\hbar$. To check that we are sweeping slowly enough, we reduced dI_{DC}/dt by a factor of two and found little difference.

[27] J.-J. Feng, Z. Huang, Z. Wang, and Q. Niu, Hysteresis from nonlinear dynamics of Majorana modes in topological Josephson junctions, Phys. Rev. B **98**, 134515 (2018).

[28] D. Averin and A. Bardas, Adiabatic dynamics of superconducting quantum point contacts, Phys. Rev. B **53**, R1705 (1996).

[29] L. Fu and C. L. Kane, Josephson current and noise at a superconductor–quantum-spin-Hall-insulator–superconductor junction, Phys. Rev. B **79**, 161408(R) (2009).

[30] S. N. Shevchenko, S. Ashhab, and F. Nori, Landau-Zener Stückelberg interferometry, Phys. Rep. **492**, 1 (2010).